08

Nanocrystalline zirconia for functional applications obtained by deposition from low-pressure arc discharge plasma

© L.Yu. Fedorov[1,2], I.V. Karpov[1,2]

[1] Federal Research Center Krasnoyarsk Scientific Center of RAS Siberian branch, Krasnoyarsk, Russia
[2] Siberian Federal University, Krasnoyarsk, Russia

E-mail: 1401-87@mail.ru

Received April 30, 2024
Revised October 28, 2024
Accepted October 30, 2024

The controlled vacuum-arc synthesis of nanoparticles and nanocrystalline layers based on zirconium dioxide ZrO_2 is considered, which allows regulating the percentage ratio of the monoclinic and tetragonal phases. The formation of the tetragonal phase is associated with the formation of a large number of oxygen vacancies formed due to high-speed quenching of nanoparticles. The samples were characterized using X-ray phase analysis. The electrical properties of the samples were studied using impedance spectroscopy and measuring the current-voltage characteristics. The dependence of the permittivity and conductivity in the direct current mode on the phase composition was established. The coexistence of the *m*- and *t*-ZrO_2 phases provides oxygen deficiency in the sample volume. This contributes to the formation of two reversible resistance states — the effect of resistive switching.

Keywords: vacuum arc, zirconium oxide, memristor, oxygen vacancies.

DOI: 10.61011/PSS.2024.12.60192.6393PA

1. Introduction

Zirconium dioxide is considered for use in nonvolatile memory devices (memory stores), and as a gate dielectric of transistors on metal oxide semiconductors [1,2]. It has good technological compatibility with silicon. When zirconium oxide is formed as thin films or nanoparticles, multiple oxygen vacancies were noted [3]. This defines its high dielectric permittivity, conductivity of *p*-type with the width of prohibited zone 5−7 eV, and the ability to form conducting channels (filaments) in the oxide structure, which provide for the possibility of resistive switching in the dielectric [4,5]. For potential inclusion of zirconium dioxide into semiconductor devices, it is important to consider in detail the mechanisms of production conditions influence at the changes of the electronic structure that are induced at the same time.

2. Experimental procedure

Nanoparticles and coatings based on ZrO_2 were synthesized in a plasma-chemical reactor described in detail in [6–8]. The reactor was first vacuumized to the basic pressure of 10^{-3} Pa. The specimens were produced at pressure of 30 and 130 Pa in the vacuum chamber with plasma-generating gas argon. Oxygen was fed into the reactor at the level of 20 vol.% of argon supply in such a way as to form a homogeneous envelope around the plasma torch.

The specimens were a layer structure of metal–dielectric–metal. The substrate was standard plates of *p*-Si (001) coated with a layer of silicon dioxide SiO_2 (thickness of ~ 500 nm). The lower electrode — layer of Pt (50 nm) and upper electrode — layer of Au (50 nm) were formed by magnetron sputtering. The dielectric layer — polycrystalline film of zirconium dioxide (ZrO_2) was formed by vacuum-arc sputtering and was controlled by the time of substrates exposure to plasma cloud. The thickness of ZrO_2 layer was ~ 100 nm.

The data of powder diffraction were obtained at room temperature with the help of diffractometer Bruker D8 Advance with a linear detector, radiation of Cu-K_α ($\lambda = 0.1540$ nm) was applied. Increment 2θ was 0.01°, the counting time — 0.2 s per increment. To analyze experimental X-ray patterns for crystalline structure detection, PDF-4+ data of the International Center of Diffraction Data (ICDD) were used.

Dielectric characteristics of the specimens were detected using impedance measurements made with the help of impedance analyzers Elins 1500 and Agilent E5061B. Electrophysical studies were carried out according to the scheme of flat capacitor on the specimens sputtered on the silicon plate with the conducting layer. A similar plate served as an upper electrode. The instrument was connected in a two-pin configuration. The actual (ε') and alleged (ε'') components of the complex dielectric permittivity were calculated using the following formulae: $\varepsilon' = Cd/(S\varepsilon_0)$, $\varepsilon'' = \varepsilon' \tan\varphi$, where C — capacitance, d — thickness of the specimen assessed in 100 nm (distance between the flat capacitor plates), S — area of the cross section, and ε_0 — dielectric permittivity of vacuum ($\varepsilon_0 = 8.85 \cdot 10^{-12}$ F/m).

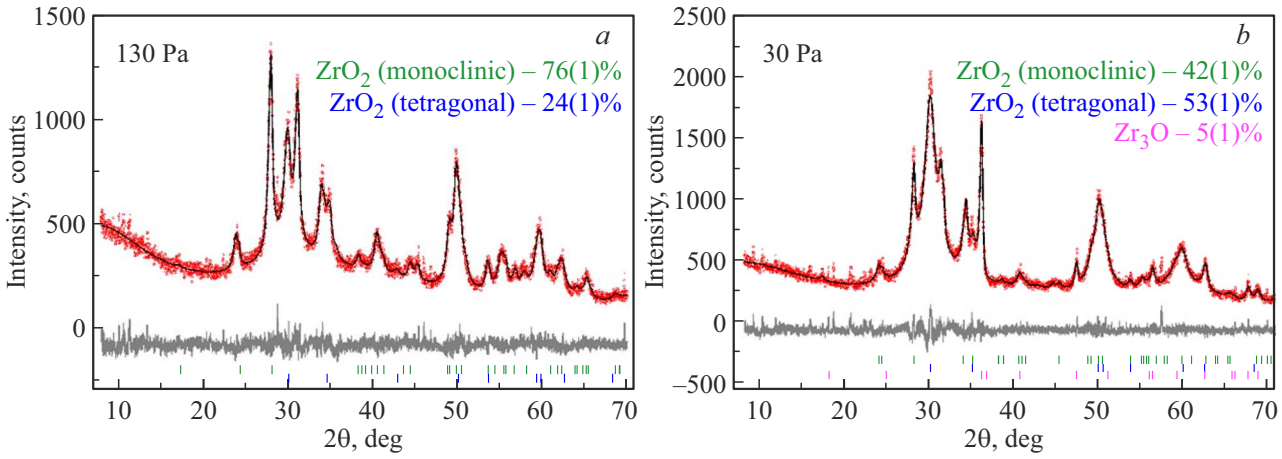

Figure 1. X-ray diffractograms of nanoparticles ZrO_2 produced at gas mix pressure of 130 Pa (*a*) and 30 Pa (*b*).

Main parameters of crystalline structure of studied specimens

Pressure during synthesis, Pa	Phase	Content, %	Group symmetry	Cell parameters: a, b, c, Å; β, deg.; volume V, Å^3	R-factors R_{wp}, R_p, χ^2
130	ZrO_2	76(1)	$P2_1/c$	$b = 5.215\,(3)$, $c = 5.327\,(3)$, $\beta = 98.90\,(1)$ $V = 142.1\,(2)$	6.60, 5.26, 1.26
	ZrO_2	24(1)	$P4_2/nmc$	$a = 3.616\,(3)$, $c = 5.173\,(4)$, $V = 67.6\,(1)$	
30	ZrO_2	42(1)	$P2_1/c$	$a = 5.153\,(5)$, $b = 5.198\,(5)$, $c = 5.325\,(5)$, $\beta = 99.08\,(2)$ $V = 140.8\,(2)$	6.32, 5.00, 1.26
	ZrO_2	53(1)	$P4_2/nmc$	$a = 3.597\,(3)$, $c = 5.193\,(4)$, $V = 67.2\,(1)$	
	Zr_3O	5(1)	$P6_322$	$a = 5.633\,(5)$, $c = 5.5211\,(4)$, $V = 143.2\,(3)$	

Electrical measurements of direct current were made using a precision source-meter Keithley 2400 in the range of 0–9 V. Electrical forming was performed at 13–15 V with the control of current flowing through the specimen.

3. Results and discussion

Diffraction patterns of specimens ZrO_2 are shown in Figure 1. The observed reflexes are related only to monoclinic and tetragonal phases ZrO_2 and Zr_3O. The obtained data were processed using the Rietveld method using TOPAS 4.2 [9] and presented in the table.

Rietveld confirmation was used for accurate definition of the specimen crystallite size. Instrumental widening of the peak was assessed using Si-standard and was further taken into account in the process of crystallite size assessment. In the specimen produced at pressure of 30 Pa, the monoclinic phase ZrO_2 has the average dimensions of the coherent scattering region (CSR) 13.1(2) nm, the tetragonal phase ZrO_2 has the average dimensions of CSR 5.4(1) nm, and in the specimen obtained at 130 Pa, — 19.0(6) nm and 8.2(2) nm accordingly.

The following features were found at frequency dependences of dielectric permittivity ZrO_2 (Figure 2). The actual part $\varepsilon'(\omega)$ of dielectric permittivity of the specimen obtained at pressure of 30 Pa, at low frequencies approaches $\sim 4 \cdot 10^4$. The alleged component demonstrates power behavior below 10^5 Hz. Besides, a relaxation peak is observed at frequency of ~ 10 Hz. Besides, the effect of transition from the state of high resistance to the state of low

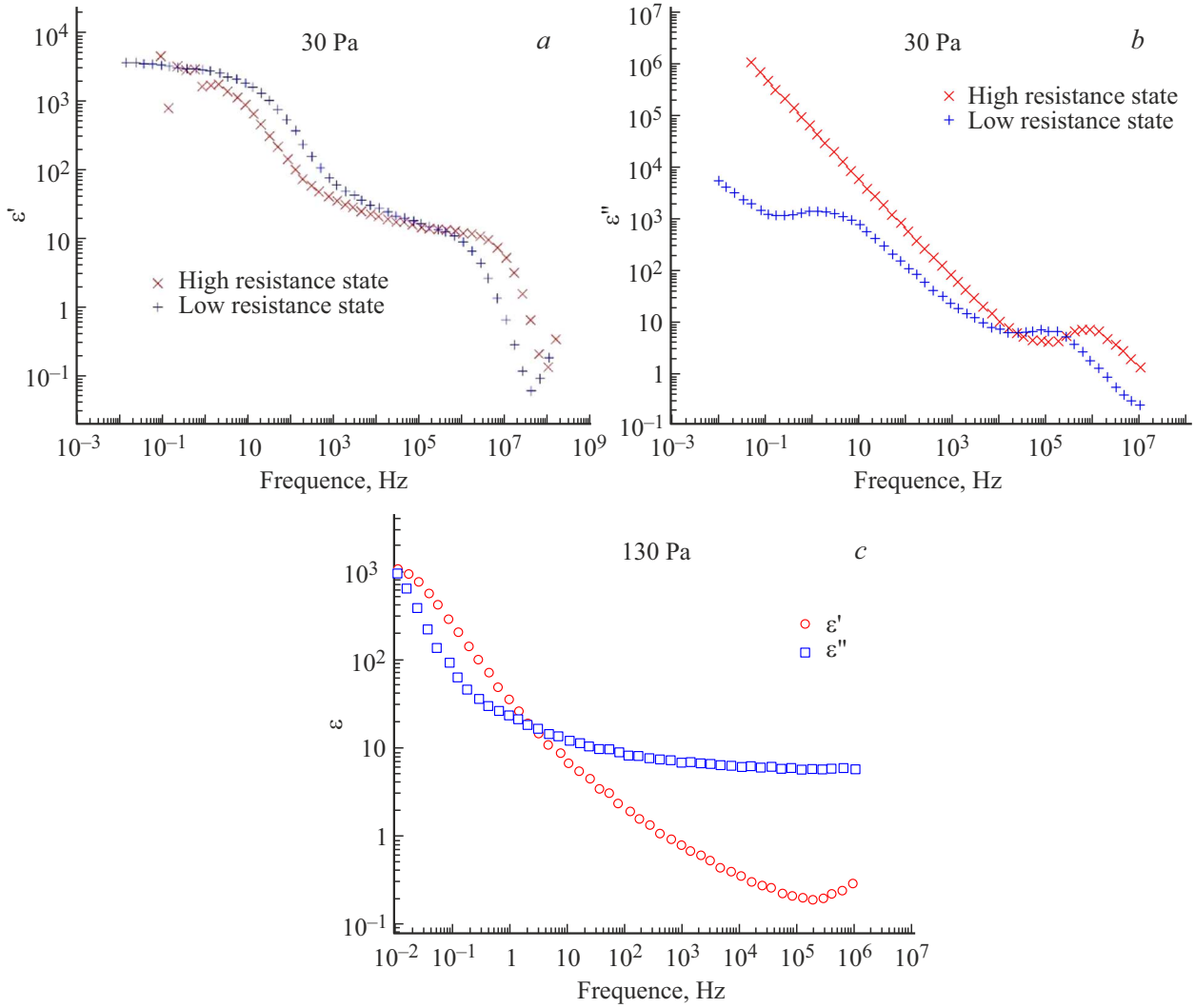

Figure 2. Actual (a) and alleged (b) components of dielectric permittivity of the specimen produced at pressure of 30 Pa, and the specimen produced at pressure of 130 Pa (c).

resistance is observed. One may separate the contribution of dielectric permittivity in the complex dielectric permittivity at DC $\varepsilon'' \propto \omega^{-1}$, as well as the relaxation peak. The specimens may have negative resistance controlled by voltage. For the specimen obtained at the pressure of 130 Pa, the dielectric permittivity ε'' reduction is observed. Besides, a small displacement of the relaxation peak towards the lower frequencies is visible. No effect of resistive switching is observed in this specimen.

Figure 3 shows the current-voltage curve of the specimens produced at 30 and 130 Pa. As one can see from the figure, in the specimen obtained at the pressure of 30 Pa, the effect of transition from the low-resistance on state to the high resistance off state) manifests itself at voltage of around +5 V. While for the specimen obtained at pressure of 130 Pa, the effect of transition is absent in the region of the instrument sensitivity.

This phenomenon is explained by the stoichiometric composition of the synthesized coatings from nanoparticles ZrO_2 and makes it possible to assume that the process of charge transport thereinto is related to localized states in the prohibited area [10]. The model that describes the effect of resistive switching in the dielectric films that is most developed at the moment, is a filamentary model based on oxygen vacancies [11]. Current-voltage curve measurements confirm that the prevalent mechanism of transport is hopping conductivity. It is found that as the oxygen-deficit phase content grows, the DC conductivity increases, and the frequency of the relaxation peak drops, which may be due to various processes of charge capturing and release. In one case the charge carriers may be excited from the Fermi level to the conduction band with higher energy. Then they are again captured by traps at Fermi level. More beneficial for the charge carriers would be the hops between the localized states in the conduction band (since they are more dense here), compared to between the traps at Fermi level.

Also a situation may arise, when the maximum of localized states density is located below Fermi level. Then

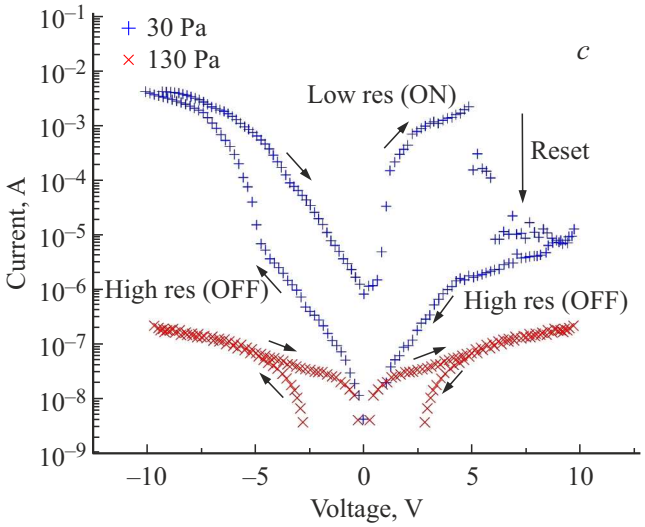

Figure 3. Current-voltage curves of specimens produced at pressure of 30 and 130 Pa.

the DC conductivity is due to the hops at the Fermi level, and the relaxation peak occurs due to the emission of the carriers to Fermi level and subsequent recapturing.

When measuring the current-voltage curve of the specimens containing the oxygen-deficit phase, the switching position is noted: they may stay in the on state with high conductivity and in the off state — with the low one. Stoichiometric specimens demonstrate no such behavior. The growth of the oxygen-deficit phase in the specimens may also lead to higher content of hydroxyl groups in the nanoparticles. This increases the quantity of electrons contributing to conductivity. As a result of Fermi level displacement towards higher energies, the probability of charge capturing and release reduces, and the frequency of relaxation peak observation drops. Stoichiometric specimens contain fewer oxygen vacancies. The conductivity of such specimens is lower due to lower density of localized states in the conduction band. It should be noted that stoichiometry by oxygen results in fewer localized states in the prohibited area.

4. Conclusion

Specimens of nanoparticles and coatings based on ZrO_2 are synthesized with various phase composition and stoichiometry. The specimen with the highest content of the tetragonal phase demonstrates the effect of switching from the high resistance state to the low resistance state. While in the specimen that mostly contains monoclinic phase, this effect is not observed. This phenomenon is explained by the presence or absence of oxygen vacancies. In the specimen with oxygen-deficit phase, the conductivity growth is observed in the DC mode, which may be due to various processes of charge capturing and release. Besides, tunneling may be observed along the path of the current flow or hops with participation of phonons between the localized states in the prohibited area. In stoichiometric specimens the conductivity is much lower due to the content of oxygen vacancies.

Funding

This study was supported financially by grant from the Russian Science Foundation No. 24-29-00374, https://rscf.ru/project/24-29-00374/

Conflict of interest

The authors declare that they have no conflict of interest.

References

[1] O.N. Gorshkov, I.N. Antonov, A.I. Belov, A.P. Kasatkin, A.N. Mikhaylov. Tech. Phys. Lett. **40**, *2*, 101 (2014). DOI: https://doi.org/10.1134/S1063785014020084.
[2] A.V. Emelyanov, K.E. Nikiruy, V.A. Demin, V.V. Rylkov, A.I. Belov, D.S. Korolev, E.G. Gryaznov, D.A. Pavlov, O.N. Gorshkov, A.N. Mikhaylov, P. Dimitrakis. Microelectron. Eng. **215**, 110988 (2019).
[3] S. Shukla, S. Seal. Int. Mater. Rev. **50**, 45 (2005). DOI: 10.1179/174328005X14267.
[4] S. Kumar, A.K. Ojha. J. Alloys Compd. **644**, 654 (2015). DOI: 10.1016/j.jallcom.2015.04.183.
[5] C.H. Lai, H.W. Chen, C.Y. Liu. Materials **9**, 551 (2016). DOI: 10.3390/ma9070551.
[6] A.V. Ushakov, I.V. Karpov, L.Yu. Fedorov, E.A. Goncharova, M.V. Brungardt, V.G. Demin. Technical Physics **67**, 2410 (2022). DOI: 10.21883/TP.2022.15.55268.157-2
[7] A.V. Ushakov, I.V. Karpov, A.A. Lepeshev, S.M. Zharkov. Vacuum **128**, 123 (2016). DOI: 10.1016/j.vacuum.2016.03.025.
[8] A.V. Ushakov, I.V. Karpov, A.A. Lepeshev, M.I. Petrov. Vacuum **133**, 25 (2016). DOI: 10.1016/j.vacuum.2016.08.007.
[9] Bruker AXS TOPAS V4: General profile and structure analysis software for powder diffraction data. User's Manual. Bruker AXS, Karlsruhe, Germany (2008).
[10] E.W. Lim, R. Ismail. Electronics **4**, 586 (2015). DOI: 10.3390/electronics4030586.
[11] M.J. Rozenberg, M.J. Sánchez, R. Weht, C. Acha, F. Gomez-Marlasca, P. Levy. Phys. Rev. B **81**, 115101 (2010). DOI: 10.1103/PhysRevB.81.115101.

Translated by M.Verenikina